Electrochimica Acta 95 (2013) 29–37

Contents lists available at SciVerse ScienceDirect

Electrochimica Acta

journal homepage: www.elsevier.com/locate/electacta

Phase-change-related degradation of catalyst layers in proton-exchange-membrane fuel cells

Gi Suk Hwang[a], Hyoungchul Kim[b], Roger Lujan[c], Rangachary Mukundan[c], Dusan Spernjak[c], Rodney L. Borup[c], Massoud Kaviany[b], Moo Hwan Kim[d], Adam Z. Weber[a,*]

[a] Environmental Energy Technologies Division, Lawrence Berkeley National Laboratory, 1 Cyclotron Road, Berkeley, CA 94720, USA
[b] Department of Mechanical Engineering, University of Michigan, Ann Arbor, MI 48109, USA
[c] Los Alamos National Laboratory, MS D429, MST-11, Los Alamos, NM 87545, USA
[d] Department of Mechanical Engineering, Pohang University of Science and Technology, Pohang, Kyungbuk 790-874, South Korea

ARTICLE INFO

Article history:
Received 19 October 2012
Received in revised form 28 January 2013
Accepted 1 February 2013
Available online xxx

Keywords:
Membrane electrode assembly (MEA)
Pt/C dispersion
Nanostructured thin film (NSTF)
Degradation
Freeze/thaw cycle
Environmental scanning electron microscope (ESEM)

ABSTRACT

Understanding and optimizing water and thermal management in the catalyst layer of proton-exchange-membrane fuel cells is crucial for performance and durability improvements. This is especially the case at low temperatures, where liquid water and even ice may exist. In this article, the durability of a traditional Pt/C dispersed and a nanostructure thin film (NSTF) membrane-electrode assembly (MEA) are examined under wet/dry and freeze/thaw cycles using both in situ and ex situ experiments. Multiple isothermal cold starts result in a performance degradation for the dispersed MEA, while no such a degradation is found in the NSTF. The results are consistent with stand-alone MEA tests, wherein the dispersed catalyst layer results in an exponential increase in the number and size of cracks until it delaminates from the membrane due to the impact of the freeze/thaw process within the catalyst-layer pores. The NSTF catalyst layer shows minimal crack generation without delamination since the ice forms on top of the layer. The results are useful for understanding degradation due to phase-change containing cycles.

1. Introduction

Proton-exchange-membrane fuel fells (PEMFC) are promising, efficient energy-conversion devices for transportation applications; however, they require optimal water and thermal management for successful commercialization [1,2]. One barrier to commercialization is the ability to start up and operate from subzero conditions where ice may exist within the porous media. The current target temperature of −20 °C (−40 °C for survivability) [3] necessitates that even if there is supercooling (where some water exists in a liquid form at subfreezing temperatures) [4,5], a significant amount of water will freeze in these circumstances. The ice is expected to impact not only cold-start success and performance, but also freeze/thaw cycles could impact durability and ultimately cause performance degradation.

At subfreezing temperatures, the produced and transported water can freeze in the cathode catalyst layer, causing blockage of available electrochemical surface area (ECSA) and possibly inducing mechanical damage due to volume expansion during freeze [6–16]. Over a PEMFC's lifetime, repeated thermal cycles between subfreezing and normal operating temperatures can lead to significant damage, especially to the cathode catalyst layer. To reduce this possible damage and enable successful cold start, the typical strategy is to remove as much water as possible during cell shutdown, thereby increasing the water capacity during startup before mass-transport limitations occur. However, this is not always possible, especially for thin-film catalyst layers, and it also results in parasitic power and fuel losses due to gas purging.

Two different canonical PEMFC catalyst layers, which are shown in Fig. 1, are used in this study. The traditional, dispersed catalyst layers are on the order of 10–20 μm thick and contain platinum nanoparticles supported on carbon (Pt/C) as the electrocatalyst and ionomer binder for proton conductivity and empty pore space to allow for efficient oxygen ingress and water egress. The nanostructured thin-film (NSTF) catalyst layer from 3 M Company on the other hand is on the order of 0.5 μm thick and does not contain ionomer, and the electrocatalyst is an extended polycrystalline Pt surface (i.e., whisker) coated on an organic support. The advantage of the NSTF catalyst layer is that its carbon-free configuration leads to mechanical/electrochemical stability, which might result in better durability, and also allows for high mass activities [17–19]. The disadvantage is that the thinner NSTF structure leads to reduced

* Corresponding author. Tel.: +1 5104866308.
E-mail address: azweber@lbl.gov (A.Z. Weber).

0013-4686/$ – see front matter © 2013 Elsevier Ltd. All rights reserved.
http://dx.doi.org/10.1016/j.electacta.2013.02.017

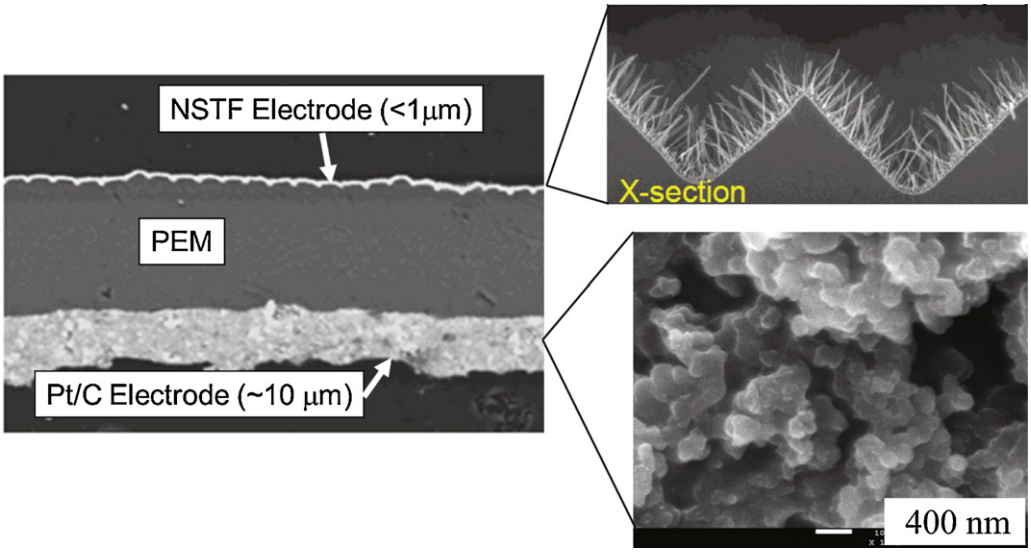

Fig. 1. Scanning electron micrographs of a cross-sectional view of a MEA with both a dispersed Pt/C and a nanostructured thin-film (NSTF) catalyst layer, including cross-sectional view of NSTF and surface view of Pt/C dispersed one.

water-holding capability and demonstrates a tendency to flood at low temperatures, which in turn result in poor transient response [20,21] and lack of cold-start robustness [22].

A number of studies have investigated MEA durability under the cyclic thermal operation at subfreezing temperatures mainly for dispersed Pt/C catalyst layers [6–8,13,23–35]. The impacts of multiple thermal cycles ($T = -40$ to 80 °C with 4 to 385 cycles) on performance have been minimal in relatively dry MEAs (i.e., purged with dry gas before freezing) [6,23–25]. However, the results for relatively wet MEAs have not been consistent. No significant performance losses were observed after 3 thermal cycles from $T = -10$ to 80 °C [26], 40 cycles from $T = -40$ to 80 °C [27], and 20 cycles from $T = -20$ to 30 °C [6]. However, in other tests only 2 to 3 cycles of isothermal cold start from a dry MEA at $T = -10$ °C resulted in apparent ECSA and performance losses [28,29]. Other experimental results under similar experimental conditions reported significant degradation for multiple freeze/thaw cycles of pre-wet MEAs with and without microporous and gas-diffusion layers (MPLs and GDLs) for 40 cycles at $T = -80$ to 80 °C [7,8,13,30,31]. These studies observed that the performance losses are caused by various factors such as reduced ECSA [6,7] and porosity [30], increased pore size [7], membrane pinholes [31], interfacial delamination [8,31], and increased contact resistance [7,13,32]. The discrepancy between no measurable degradation and significant performance/physical degradation with thermal cycles in existing studies can be associated with the different experimental protocols, MEA manufacturing processes, and/or cell assemblies, which potentially could impact the water and mechanical-stress distributions throughout the catalyst layers. For example, freezing of pre-wet MEAs is expected to be more gradual compared to that of the produced water at the cathode catalyst layer during an isothermal cold start. In addition, the degree of the degradation is related to the amount of the residual water in the adjacent layers, i.e., membrane and MPLs/GDLs, which may provide different stress distribution by different volume expansion, including upon cell assembly [8,33]. The cooling rate and different GDL types (paper and cloth) including different PTFE loadings might also have influenced the performance degradation [34,35].

Compared to the typical dispersed Pt/C catalyst layers, freeze-related degradation with NSTF catalyst layers has been much less studied. A few studies have shown that mechanical and electrochemical degradation were reduced [17,18], since it is carbon and ionomer free, but the exact origins require further exploration. Furthermore, all of the above studied were in situ and utilized full cells, which inhibits exploration of the nature of the possible freeze-related damage.

In this study, the impact of cold start in terms of physical and performance changes is investigated through both in- and ex situ studies. In particular, the propensity for the catalyst layer to crack upon water phase changes and the crack generation/evolution are visualized using novel environmental scanning electron microscopy (ESEM) studies. Both dispersed and NSTF MEAs are utilized and tested both in cyclic passive cooling and isothermal cold starts at −10 °C. The degree of degradation is measured in terms of the polarization performance, ECSA, and crack surface density.

2. Experimental

2.1. Samples

Dispersed Pt/C MEAs were obtained from Ion Power Inc., with nominal catalyst loadings of 0.3 mg_{Pt}/cm^2 with VulcanXC72R carbon and Nafion® 1100 g/mol equivalent weight (EW) ionomer binder and Nafion® 115 membrane. NSTF MEAs were provided by 3 M Company and contained 0.1 mg_{Pt}/cm^2 with 3 M 800 EW membrane. For the single-cell fuel cell test of the dispersed catalyst, the anode was a 20%Pt/Vulcan XC72 carbon and the cathode was a 40%Pt/EA-carbon, and the NSTF was 0.15 mg_{Pt}/cm^2 at the cathode and 0.05 mg_{Pt}/cm^2 at the anode.

2.2. Environmental scanning electron microscopy

Environmental scanning electron microscopy (ESEM) is a useful tool to understand surface water behavior in various PEMFC components due to high spatial resolution in a humidity-controlled environmental chamber [36–38]. However, those studies have primarily focused on condensation and liquid-water transport. Here, ESEM (FEI Quanta 200 at the University of Michigan) was extensively used to investigate water behavior under subfreezing temperature and its impact on durability. The state of water was controlled by the water vapor pressure and temperature using a vacuum pump and Peltier cooling stage. The MEAs were placed on the temperature-controlled aluminum sample holder as shown

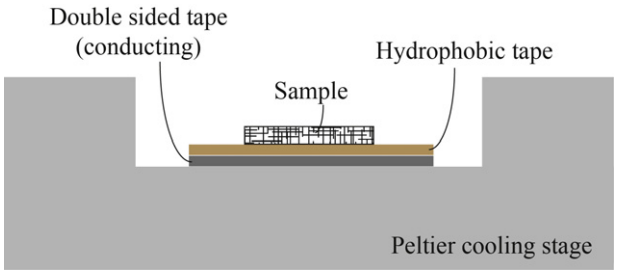

Fig. 2. Schematic of the ESEM experimental setup. The MEA samples are placed on the aluminum sample holder. Peltier cooling stage, hydrophobic tape, and thermal/electrical conducting tapes placements are also shown.

in Fig. 2, and a hydrophobic tape (PTFE) was applied to avoid invasion of condensed water from the sample edge. A thermal/electrical conducting tape was also placed to minimize thermal contact resistance for careful sample temperature control. The built-in thermocouple of the Peltier cooling controller was calibrated using a separate thermometer (OMEGA, 450AET). The operating temperature and pressure ranges were $T = -12$ to 12 °C and $p_v = 0.08$ to 5 torr.

The electron beam was used only when taking images to minimize beam damage. The exposure time per image was typically 1 min, and during the cyclic operation, the total exposure time was about 10–20 min depending on the number of cycles. To confirm the minimal beam damage, both the dispersed and NSTF MEAs were exposed to the irradiation for 20 min without thermal cycles and no apparent damage (cracking) was observed (not shown).

To mimic the water behavior for the freezing/thawing and condensing/evaporating process during typical PEMFC start-up/shut-down procedures, three cyclic pathways were chosen, i.e., liquid to ice (path 1), vapor to liquid (path 2), and vapor to ice (path 3) as shown in Fig. 3(a). One cycle took 12 min, and the maximum number of cycles was 20. The water condensation and freezing/thawing created morphology/texture changes (ice appears rougher than liquid water), as detected by observation. Similarly, cracks were detected by visual inspection at 2000× magnification and counted per given surface area, which was used as a metric for degree of surface degradation,

$$\tilde{n}_{d,A} = \frac{n_{c,A}}{n_t} \quad (1)$$

where $n_{c,A}$ is the number of cracked regions per image area and n_t is the total number (30) of subsections in the image (5×6). The onset of water condensation on the MEA surfaces is shown in Fig. 3(b) along with a hydrophilic substrate (i.e., aluminum foil). The phase diagram validates the use of visual inspection of the water droplet and associated morphological changes to predict freezing. From the figure, both catalyst layers appear hydrophilic.

2.3. Fuel-cell testing, characterization, and post-test analyses

Both passive thermal cycling and isothermal starts were conducted in single-cell fuel cells using a fuel-cell test station (Fuel Cell Technologies) for both the dispersed and NSTF catalyst layers. For the former, SGL 25BC diffusion media were used; for the latter, diffusion media were provided by 3 M Company. For the isothermal cold starts, cells were run at −10 °C at a constant current of 0.02 A/cm^2 until the cell potential degraded to 0 V due to transport limitations. For the passive thermal cycling, 50 cm^2 fuel cell assemblies with a quad-serpentine flow field were run at 80 °C and then brought down to −10 °C for half hour and then back up to +10 °C. After every 5 isothermal starts or passive thermal cycles, polarization curves were recorded at 80 °C, 63% inlet relative humidity, and hydrogen and air stoichiometries of 2 and 2.5,

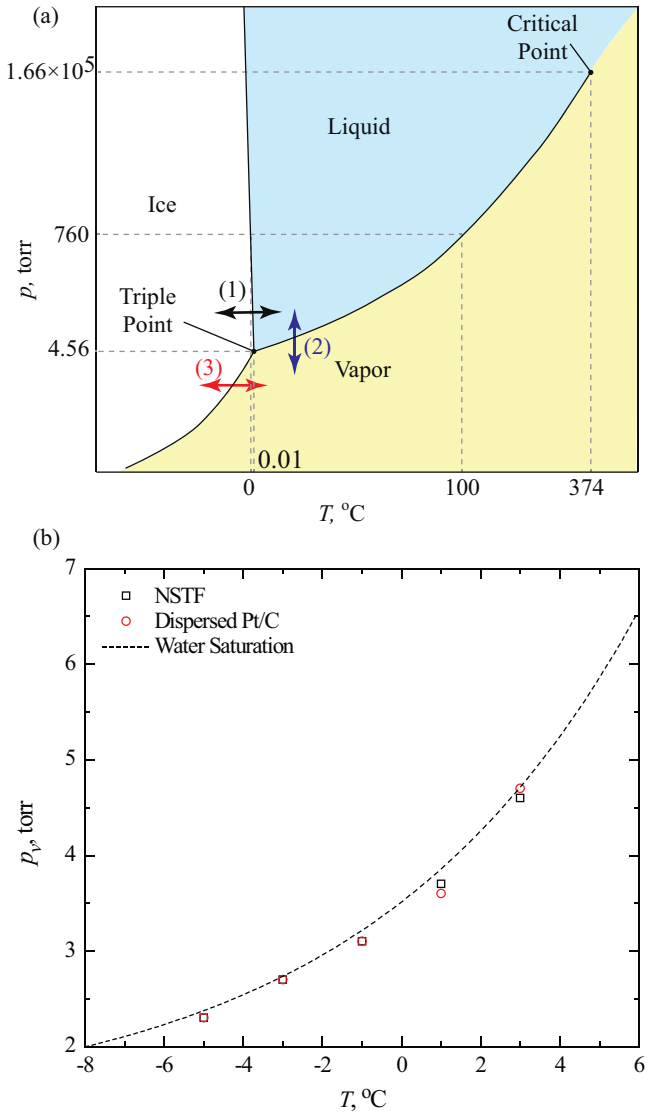

Fig. 3. (a) Phase diagram for water showing the three cyclic ESEM paths used in the experiments. (b) Onset of water condensation for the two catalyst layers, also shown is the aluminum foil phase diagram for reference.

respectively. Similarly, the ECSA was periodically measured using cyclic voltammetry (from 0.085 to 1.0 V vs. RHE at a scan rate of 100 mV s^{-1}) and calculated from the average of the hydrogen desorption/adsorption peaks after correction for baseline and electrode capacitance. In addition, the mean Pt particle size of virgin catalyst powders and those removed from tested MEAs (i.e., after 20 cycles) were measured using X-ray diffraction (XRD) (Siemens D5000, Cu k-α radiation). The XRD data were fit using whole-pattern fitting methods (Shadow analysis software by MDI Inc.) with particle-size and strain-line-broadening functions [39]. We also employed micro X-ray computed tomography (microXCT) to visualize changes in the internal morphology of the MEAs before and after in situ temperature cycling. Tomographic image sets of new and tested MEAs were recorded by a MicroXCT system (Xradia, Inc.) with a field of view of 1 by 1 mm and a resolution of ~2 μm.

3. Results and discussions

3.1. In situ freeze/thaw cycling and cell performance

As mentioned above, the NSTF catalyst layer is expected to have a substantially lower water-holding capacity than that of the

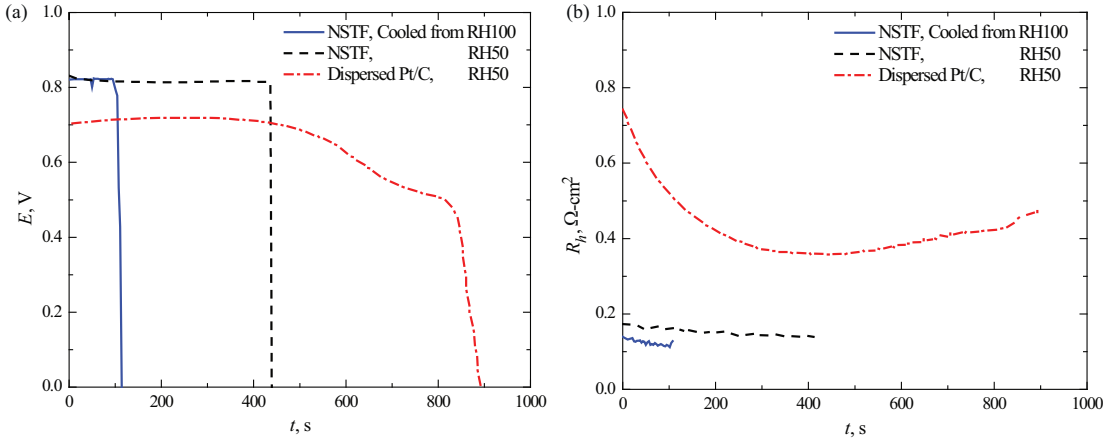

Fig. 4. (a) Measured performance, and (b) high frequency resistance, R_h, as a function of time during the isothermal cold start at −10 °C, 0.02 A/cm^2 for NSTF and dispersed Pt/C catalyst layers at different starting relative humidities (RHs).

dispersed catalyst layer. This lower capability is observed from an isothermal start as shown in Fig. 4(a). Interestingly, the measured water capacity during the cold start (2 and 9 C/cm^2 for 50% and 100% RH, respectively) is higher than the intrinsic capacity of the layer (~0.2 C/cm^2), indicating that water moves away from the NSTF layer during the isothermal freeze at −10 °C, where it is thought that freeze kinetics are nucleation limited [4,5]. This extra capacity is observed even under fully humidified conditions, where it is expected that the membrane can no longer act as a storage medium for the generated water (see the difference between the two NSTF curves in Fig. 4) [22].

To understand the impact of the freeze on cell resistance, Fig. 4(b) shows the high-frequency resistance obtained from impedance during the isothermal cold start. The NSTF exhibits a

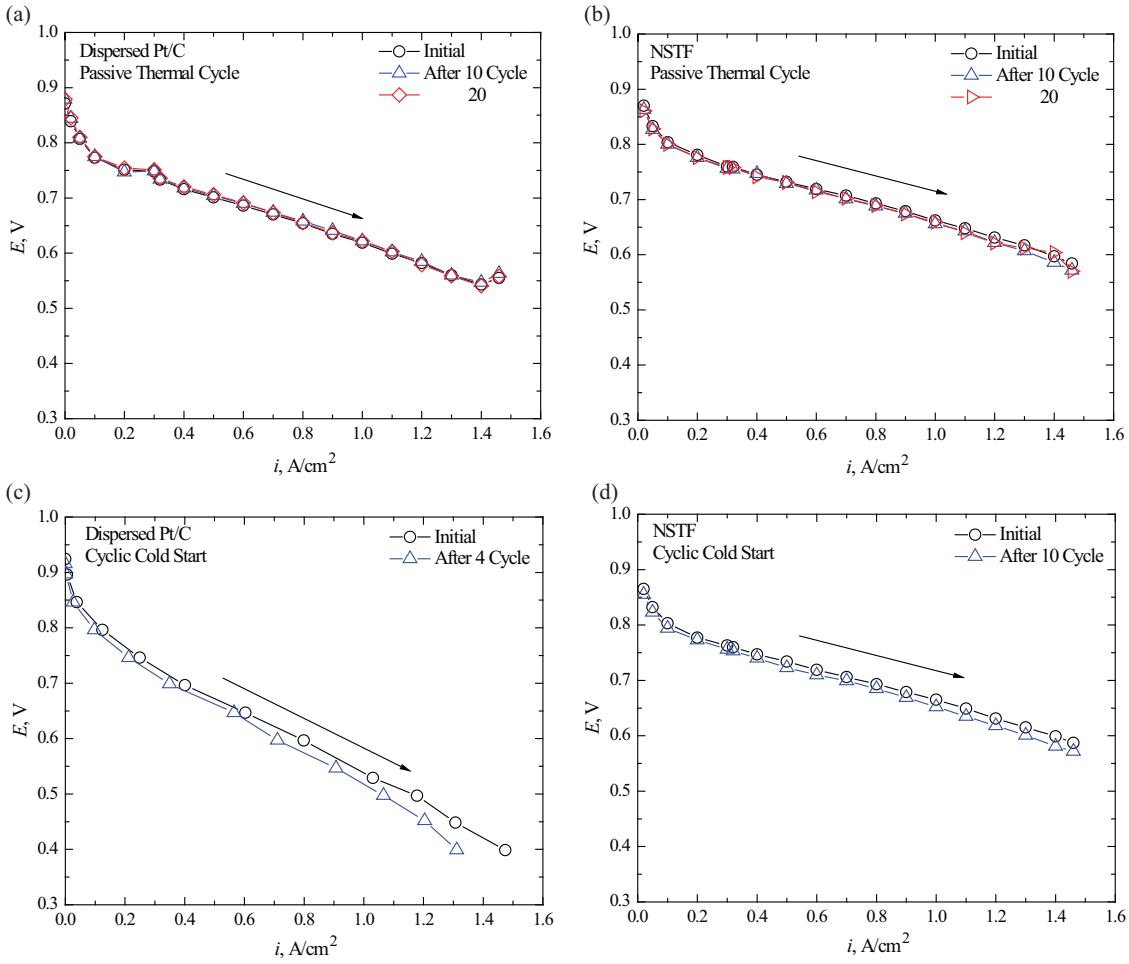

Fig. 5. Polarization curves after 0 (initial), 10, and 20 passive thermal cycles for (a) dispersed Pt/C and (b) NSTF MEAs. Polarization curves, (c) for dispersed Pt/C MEA after 0 and 4 isothermal cold starts and (d) for NSTF MEA after 0 and 10 isothermal cold starts at −10 °C.

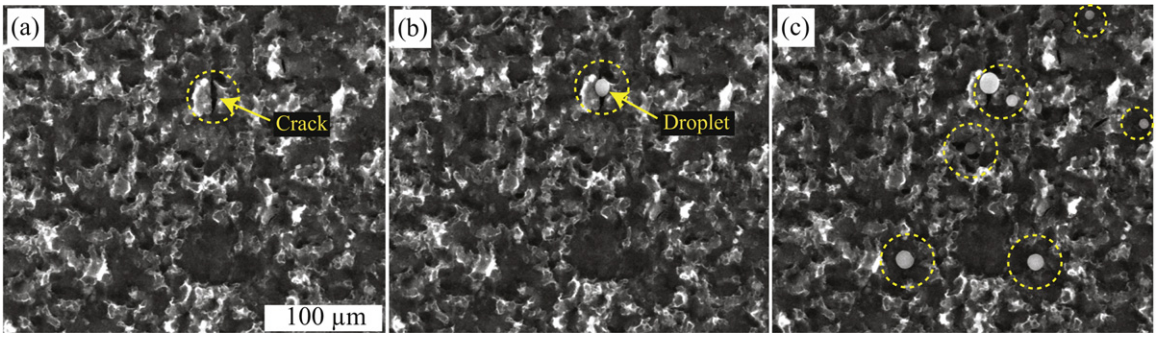

Fig. 6. ESEM time-series images of the dispersed Pt/C catalyst layer, (a) no condensation, (b) preferential condensation of water droplet within a crack, (c) subsequent and oozing out and condensation in the other locations.

smaller resistance, which may be due to the thinner membrane, and a resistance that is independent of current density. The increasing resistance with current density for the dispersed Pt/C may be due to ice crystals isolating and separating the carbon particles within the catalyst layer. However, for the NSTF, ice will form on the surface of the backing layer and spread, and thus a concern would be delamination of the diffusion media due to ice formation. Since the high-frequency resistance is constant, this is not expected to occur under these conditions.

Fig. 5 shows the impact of both the passive thermal cycles and the cyclic isothermal starts for the two types of catalyst layers. The passive thermal cycled cells show no appreciable change in performance (although subsequent passive cycles down to −40C did show a few percent performance decrease), which is attributed to perhaps some liquid (unfrozen) water remaining at the minimum temperature of −10 °C after the 1 h cool down and 30 min hold [5]. In addition, there may be minimal impact since there could be a small amount of water within the micropores of the catalyst layer since the method of wetting the MEA depends on operating the cell and cooling it down. In contrast, the isothermal starts generate water within the catalyst layer (catalytic sites), resulting in more ice within the micropores. This is observed as shown in Fig. 6, where the ESEM images clearly show water preferentially condensing and existing within the crack or pore. Fig. 5(c) and (d) clearly shows that for the dispersed MEA, the performance appreciably decreases after the cyclic isothermal cold starts, whereas the NSTF MEA does not exhibit a substantial change in performance.

To further investigate this issue, the ECSA was determined. For the dispersed MEA, the ECSA decreased from 86 to 59 cm^2/cm^2 after the passive thermal cycles, and the mean Pt particle size increased from 2.2 to 2.6 nm for the anode and 3.8 and 5.1 nm for the cathode. These results are qualitatively consistent with the decrease in performance (see Fig. 5(c)), and indicate that some morphological changes occur within the catalyst layer due to the freezing process. For the NSTF, the ECSA increased from 6.7 to 10 cm^2/cm^2, which may be indicative of the freeze/thaw helping to condition the cell and possibly fracture the underlying support. While the NSTF does not have high water capacity, it does demonstrate improved freeze\thaw and subzero temperature durability compared to the traditional Pt/C dispersed catalyst layer.

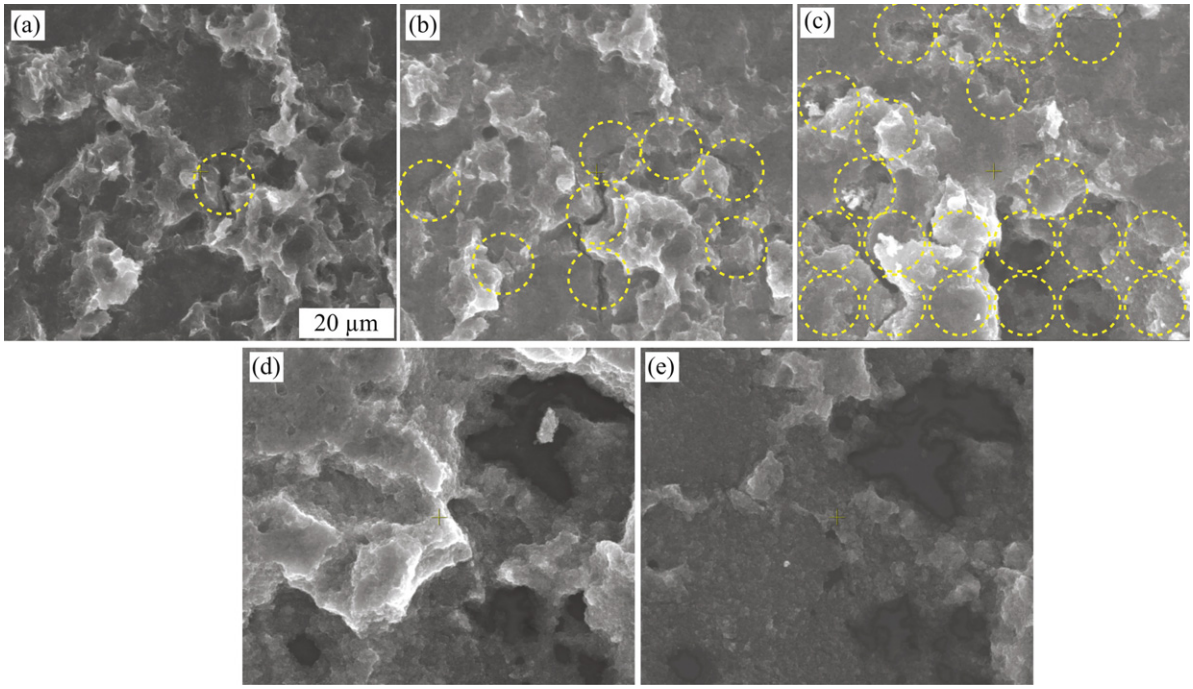

Fig. 7. ESEM images of dispersed Pt/C MEA (a) as received and after (b) 5, (c) 10, (d) 15, and (e) 20 liquid/ice cycles, path(1) in Fig. 3(a). The dotted lines are marked to highlight crack locations within the circle area.

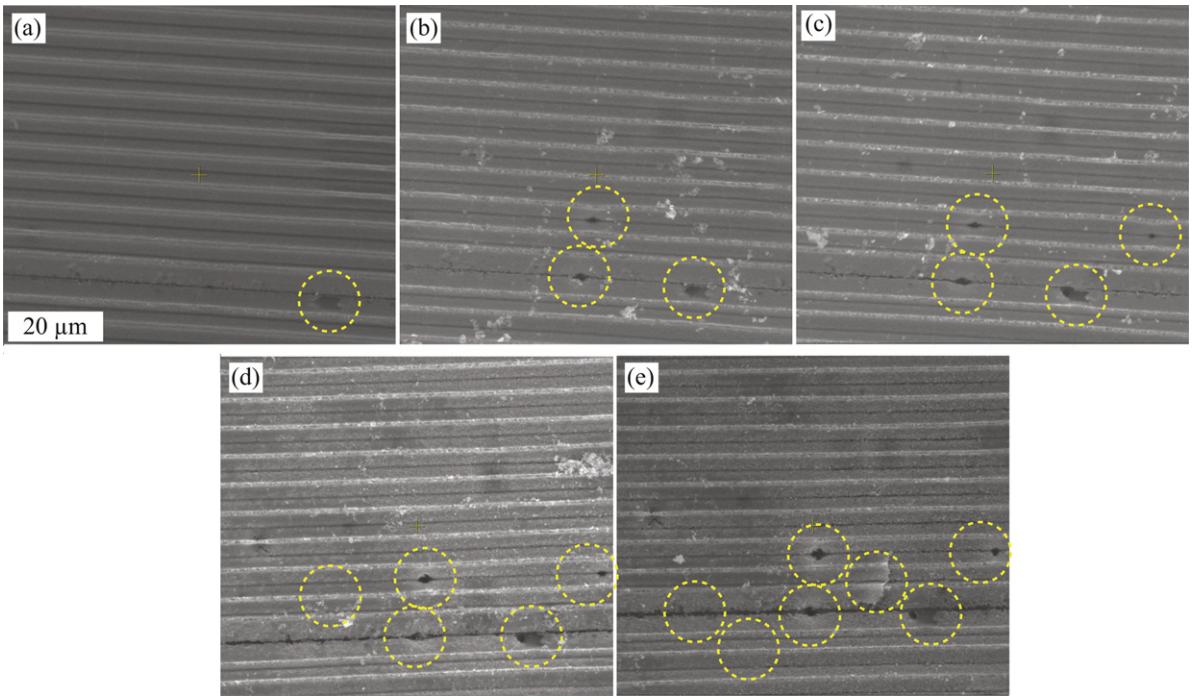

Fig. 8. ESEM images of NSTF (a) as-received and after (b) 5, (c) 10, (d) 15, and (d) 20 liquid/ice cycles, path(1) in Fig. 3(a). The dotted lines are marked to highlight crack locations within the circle area.

3.2. Environmental scanning electron microscopy

To explore phase-change-related degradation mechanisms further, cycling studies were conducted using the ESEM. The generation and evolution of the cracks under water freeze/thaw cycles (liquid/ice, path (1) in Fig. 3(a)) are visualized in Fig. 7 for the dispersed catalyst layer. In the intact sample, minimal cracks are found, and the number of cracks increases as the number of cycles increases, until significant delamination of the layer from the membrane occurs after 15 cycles. It is clear that the observed changes are much more damaging than those suggested by the in situ cell performance changes; this indicates that the ex situ conditions are perhaps more severe or the cell assembly and diffusion media help to provide support and minimize the impact of freeze [8]. In addition, unlike the in situ test, the water is generated by local condensation instead of capillary flow from the adjacent layers. Nonetheless, the qualitative trend is consistent with the above mentioned in situ performance and observed ECSA changes, i.e., water freezing results in appreciable morphological changes within the catalyst layer.

In the NSTF catalyst layers, phase and thermal cycling do not significantly impact the structure, as seen in Fig. 8. Although some cracks seem to form at the valley of the zig-zag structure, they are isolated and may be caused by beam damage as well as ice formation or swelling stresses by the membrane, and delamination does not occur even after 20 cycles. Thus, similar to the in situ performance, the NSTF demonstrates remarkable stability under the harsher phase-change conditions within the ESEM. The phase change on the NSTF is expected to occur along the longitudinal structures (cross section shown in Fig. 1) in contrast to condensation within the pores and cracks in a dispersed catalyst layer (see Fig. 6) in the ESEM experiments. This formation place combined with the inherently stronger mechanical properties afforded by the NSTF structure improve its robustness.

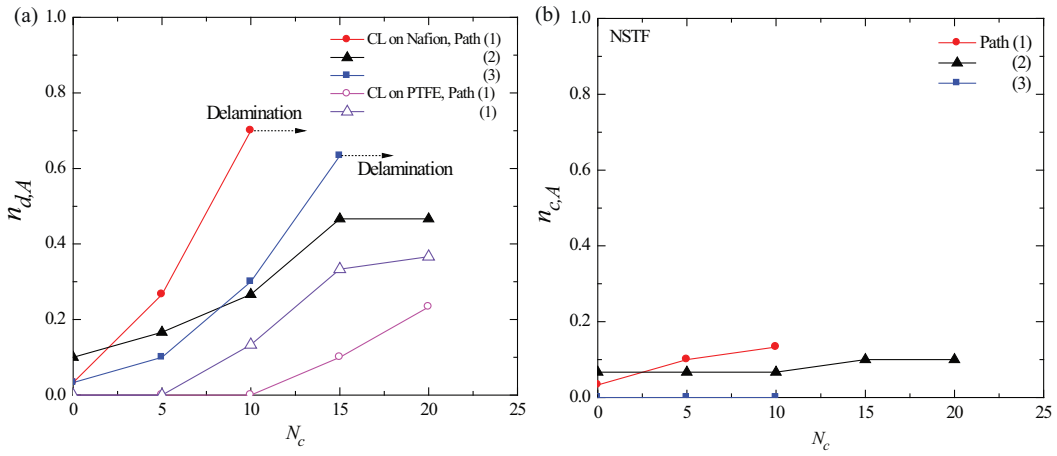

Fig. 9. Variations of the number of cracks as a function of cycle for the (a) dispersed and (b) NSTF MEAs. The results of the dispersed catalyst layer coated on PTFE are also shown in (a).

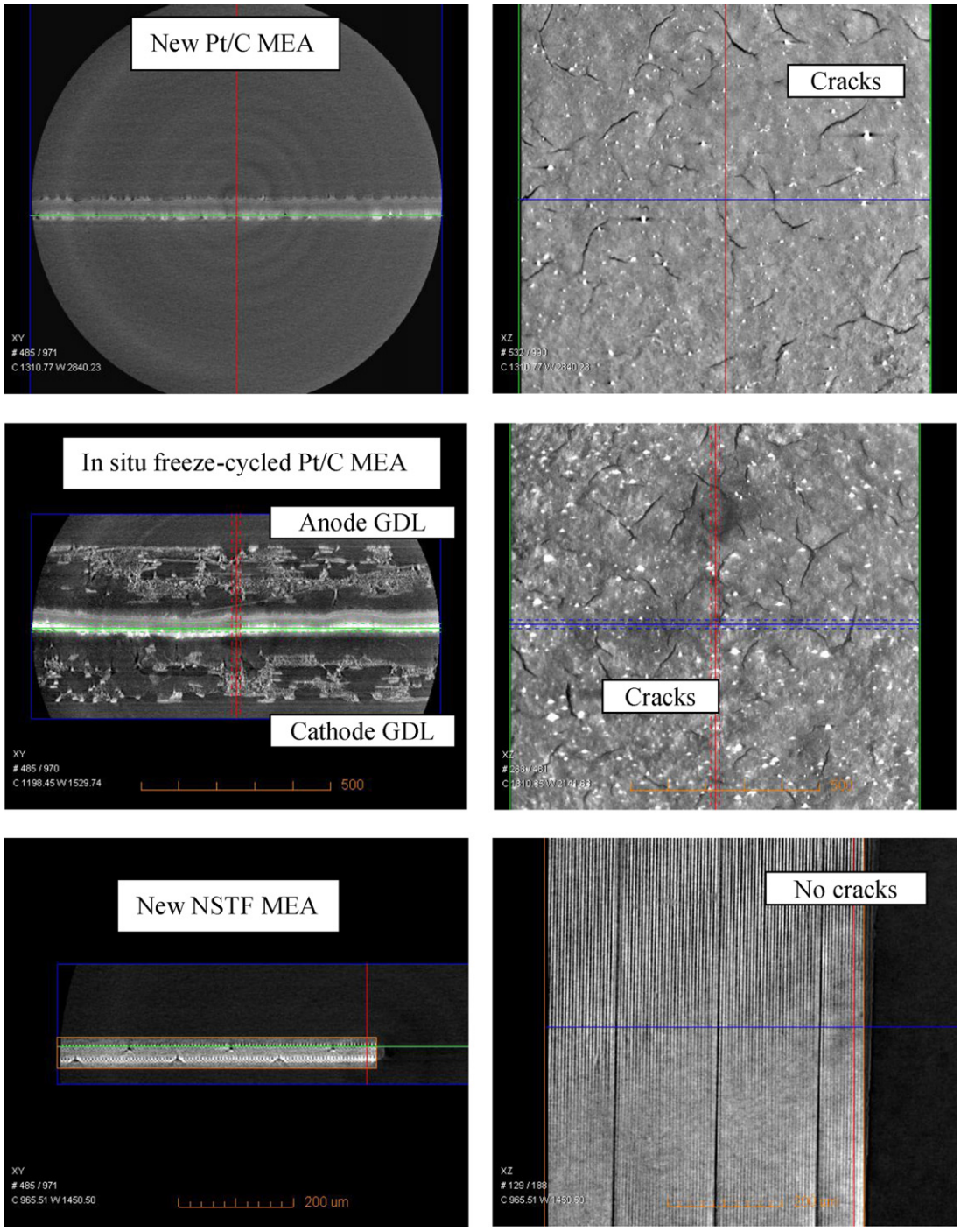

Fig. 10. Computed X-ray tomography images of the MEAs after 10 passive thermal cycles in situ. Left: MEA cross-sectional images. Right: slices showing the catalyst layer structure.

To explore the cycle impacts and quantify the cracking, Fig. 9 shows the crack surface density calculated by Eq. (1) for the different MEAs. The NSTF samples do not exhibit total failure and the crack formation and growth rates are similarly minimal for all paths. For the Pt/C dispersed catalyst layers, the normalized crack number rapidly increases as the freezing cycle number increases, and paths (1) and (3) (see Fig. 3(a)) show total failure (delamination) above 10 and 15 cycles, respectively, whereas path (2) does not demonstrate severe cracking. This suggests that the ice formation that occurs with the other paths causes more damage than the swelling/contracting of the ionomer and underlying membrane, although the membrane swelling/contracting may also play a role in NSTF cracking.

To explore the last point in more detail, ESEM cycling studies were conducted with dispersed catalyst layers on a PTFE (i.e., hydrophobic) membrane rather than Nafion® to minimize impacts of hydroscopic membrane swelling. Fig. 9 shows that it decreased the onset of cracking, although the cracking still increases rapidly once initiated with an almost exponential shape. This delay may be caused by the substrate hydrophobicity as well as the lack of membrane dimensional changes due to swelling/contracting. In addition, Fig. 9 highlights that any defects or damage within the

catalyst layer could be exacerbated and quickly propagated by freeze\thaw cycles. The results are consistent with a suggestion that formation of ice within the catalyst layer results in measurable morphological changes and subsequent decrease in surface area due to crack formation.

Finally, as discussed, the ESEM results seem to be more aggressive than those in situ, and one can wonder whether cracking will occur within assembled PEMFCs. To this end, computed X-ray tomography (XCT) of the Pt/C dispersed and the NSTF MEAs was accomplished before and after passive thermal cycling (Fig. 10). The results, as shown in Fig. 10, demonstrate that cracks exist in the Pt/C catalyst layers, both before and after testing in situ. While the XCT provides insight into the MEA's 3D structure (Fig. 10, left) with a relatively large field of view (1 mm × 1 mm), sub-micrometer features cannot be discerned due to the limited resolution of the imaging equipment. Note that the cracks shown in Fig. 10 for Pt/C cathode catalyst layers propagate throughout the catalyst-layer thickness (from the outer surface facing the MPL, to the inner interface with the membrane). These cracks are at least several micrometers wide and tens of micrometers long, and do not grow substantially over the course of 10 passive thermal cycles (see Fig. 10). One should not confuse these cracks with the ones discussed in the ESEM experiments (Fig. 7), which are more than an order of magnitude smaller and do not propagate through the entire thickness of the catalyst layer (unless complete delamination occurs). The NSTF MEA shows ordered and uniformly dispersed catalyst, without larger cracks for both new and cycled MEAs. Some minor variations in the Pt distribution after cycling, Fig. 10 bottom right, are not due to freeze cycling but rather from some of the catalyst being stuck to the MPL which was removed prior to taking the images. Post-mortem SEM analysis of in situ cycled NSTF MEAs did not reveal formation of sub-micron cracks which were formed during the ESEM experiments. Thus, the ESEM thermal cycling protocols seem to be more aggressive than those in situ, as both the Pt/C and the NSTF catalyst layers exhibited cracking on a micro-scale in the ESEM setup. Additional experiments are under way to investigate the formation and growth of both larger and sub-micrometer cracks after more severe thermal-cycling protocols within a fuel-cell assembly.

4. Summary

The impact of phase-change cycles (liquid/vapor and ice/liquid) for Pt/C dispersed and nanostructured-thin-film (NSTF) membrane-electrode-assemblies was elucidated from various observations and experimental results. Isothermal cold starts demonstrated loss of electrochemical active surface area and a decrease in cell performance for the dispersed catalyst layer, whereas the NSTF catalyst layer did not exhibit these changes. Under passive thermal cycles down to −10 °C, neither layer exhibited appreciable performance changes. For the dispersed catalyst layer, the loss in surface area was consistent with ex situ analysis of freeze/thaw cycles using an environmental scanning electron microscope (ESEM), which demonstrated crack formation and crack-density increase with cycle number due to water condensation and freezing between secondary carbon particles. The formation of ice along the NSTF structures did not result in any significant cracking of the layer, nor was delamination of the layer observed or implied from either the ESEM or in situ resistance measurements. In addition, it was shown that large catalyst-layer cracks exist after cell assembly and testing in dispersed electrodes. The findings help elucidate degradation mechanisms and effects due to phase-change cycling.

Acknowledgements

We are thankful to Dr. John Mansfield at the electron microbeam analysis laboratory, the University of Michigan (UM), for useful discussions and help with the ESEM experimental setup, and also thank Mr. Charles Endouard (ENSEEIH, Toulouse, France) for the ESEM measurement as a summer intern student at UM. This work was supported by the Assistant Secretary for Energy Efficiency and Renewable Energy, Fuel Cell Technologies Office, of the U.S. Department of Energy (contract number DE-AC02-05CH11231 for LBNL). This work is also partially supported by the sponsorship of Global Partnership Program from Ministry of Science and Technology, South Korea.

References

[1] C.Y. Wang, Fundamental models for fuel cell engineering, Chemical Reviews 104 (2004) 4727.
[2] A.Z. Weber, J. Newman, Modeling transport in polymer-electrolyte fuel cells, Chemical Reviews 104 (2004) 4679.
[3] U.S. Department of Energy, Fuel cell technologies program multi-year research. development and demonstration plan, 2012, p. 3.4 - 17.
[4] T.J. Dursch, M.A. Ciontea, C.J. Radke, A.Z. Weber, Isothermal ice crystallization kinetics in the gas-diffusion layer of a proton-exchange-membrane fuel cell, Langmuir 28 (2012) 1222.
[5] T.J. Dursch, M.A. Ciontea, G.J. Trigub, C.J. Radke, A.Z. Weber, Pseudo-isothermal ice-crystallization kinetics in the gas-diffusion layer of a fuel cell from differential scanning calorimetry, International Journal of Heat and Mass Transfer 60 (2013) 450.
[6] Q.H. Guo, Z.G. Qi, Effect of freeze-thaw cycles on the properties and performance of membraneelectrode assemblies, Journal of Power Sources 160 (2006) 1269.
[7] E.A. Cho, J.J. Ko, H.Y. Ha, S.A. Hong, K.Y. Lee, T.W. Lim, I.H. Oh, Characteristics of the PEMFC repetitively brought to temperatures below 0 degrees C, Journal of the Electrochemical Society 150 (2003) A1667.
[8] S. Kim, M.M. Mench, Physical degradation of membrane electrode assemblies undergoing freeze/thaw cycling: Micro-structure effects, Journal of Power Sources 174 (2007) 206.
[9] R.J. Balliet, J. Newman, Cold start of a polymer-electrolyte fuel cell i. development of a two-dimensional model, Journal of the Electrochemical Society 158 (2011) B927.
[10] L. Mao, C.Y. Wang, Analysis of cold start in polymer electrolyte fuel cells, Journal of the Electrochemical Society 154 (2007) B139.
[11] K. Tajiri, Y. Tabuchi, C.Y. Wang, Isothermal cold start of polymer electrolyte fuel cells, Journal of the Electrochemical Society 154 (2007) B147.
[12] J. Meyers, Subfreezing phenomena in polymer electrolyte fuel cells, in: F. Büchi, M. Inaba, T. Schmidt (Eds.), Polymer Electrolyte Fuel Cell Durability, Springer, New York, 2009, p. 369.
[13] J. Je, J. Kim, M. Kaviany, S.Y. Son, M. Kim, X-ray tomography of morphological changes after freeze/thaw in gas diffusion layers, Journal of Synchrotron Radiation 18 (2011) 743.
[14] Y. Ishikawa, T. Morita, K. Nakata, K. Yoshida, M. Shiozawa, Behavior of water below the freezing point in PEFCs, Journal of Power Sources 163 (2007) 708.
[15] Y. Ishikawa, H. Harnada, M. Uehara, M. Shiozawa, Super-cooled water behavior inside polymer electrolyte fuel cell cross-section below freezing temperature, Journal of Power Sources 179 (2008) 547.
[16] S.H. Ge, C.Y. Wang, In situ Imaging of liquid water and ice formation in an operating PEFC during cold start, Electrochemical and Solid-State Letters 9 (2006) A499.
[17] M.K. Debe, A. Schmoeckel, S. Hendricks, G. Vernstrom, G. Haugen, R. Atanasoski, Durability aspects of nanostructured thin film catalysts for PEM fuel cells, ECS Transactions 1 (2006) 51.
[18] M.K. Debe, A.K. Schmoeckel, G.D. Vernstrom, R. Atanasoski, High voltage stability of nanostructured thin film catalysts for PEM fuel cells, Journal of Power Sources 161 (2006) 1002.
[19] M.K. Debe, Electrocatalyst approaches and challenges for automotive fuel cells, Nature 486 (2012) 43.
[20] A. Kongkanand, P.K. Sinha, Load transients of nanostructured thin film electrodes in polymer electrolyte fuel cells, Journal of the Electrochemical Society 158 (2011) B703.
[21] A. Kongkanand, M. Dioguardi, C. Ji, E.L. Thompson, Improving operational robustness of NSTF electrodes in PEM fuel cells, Journal of the Electrochemical Society 159 (2012) F405.
[22] R.J. Balliet, J. Newman, Cold-Start modeling of a polymer-electrolyte fuel cell containing an ultrathin cathode, Journal of the Electrochemical Society 158 (2011) B1142.
[23] R.C. McDonald, C.K. Mittelsteadt, E.L. Thompson, Effects of deep temperature cycling on nafion (R) 112 membranes and membrane electrode assemblies, Fuel Cells 4 (2004) 208.

[24] J.B. Hou, H.M. Yu, S.S. Zhang, S.C. Sun, H.W. Wang, B.L. Yi, P.W. Ming, Analysis of PEMFC freeze degradation at-20 degrees C after gas purging, Journal of Power Sources 162 (2006) 513.
[25] E.A. Cho, J.J. Ko, H.Y. Ha, S.A. Hong, K.Y. Lee, T.W. Lim, I.H. Oh, Effects of water removal on the performance degradation of PEMFCs repetitively brought to < 0 degrees C, Journal of the Electrochemical Society 151 (2004) A661.
[26] M.S. Wilson, J.A. Valerio, S. Gottesfeld, Low platinum loading electrodes for polymer electrolyte fuel-cells fabricated using thermoplastic ionomers, Electrochimica Acta 40 (1995) 355.
[27] R. Mukundan, Y.S. Kim, F.H. Garzon, B. Pivovar, Freeze/thaw effects in pem fuel cells, ECS Transactions 1 (2006) 403.
[28] M. Oszcipok, M. Zedda, D. Riemann, D. Geckeler, Low temperature operation and influence parameters on the cold start ability of portable PEMFCs, Journal of Power Sources 154 (2006) 404.
[29] M. Oszcipok, D. Riemann, U. Kronenwett, M. Kreideweis, M. Zedda, Statistic analysis of operational influences on the cold start behaviour of PEM fuel cells, Journal of Power Sources 145 (2005) 407.
[30] J. Li, S. Lee, J. Roberts, Ice formation and distribution in the catalyst layer during freeze-start process-CRYO-SEM investigation, Electrochimica Acta 53 (2008) 5391.
[31] Q.G. Yan, H. Toghiani, Y.W. Lee, K.W. Liang, H. Causey, Effect of sub-freezing temperatures on a PEM fuel cell performance, startup and fuel cell components, Journal of Power Sources 160 (2006) 1242.
[32] R. Mukundan, R. Lujan, J.R. Davey, J.S. Spendelow, D.S. Hussey, D.L. Jacobson, M. Arif, R. Borup, Ice formation in PEM fuel cells operated isothermally at sub-freezing temperatures, ECS Transactions 25 (2009) 345.
[33] S. Kim, B.K. Ahn, M.M. Mench, Physical degradation of membrane electrode assemblies undergoing freeze/thaw cycling: Diffusion media effects, Journal of Power Sources 179 (2008) 140.
[34] R. Mukundan, Y.S. Kim, T. Rockward, J.R. Davey, B. Pivovar, D.S. Hussey, D.L. Jacobson, M. Arif, R. Borup, Performance of PEM fuel cells at sub-freezing temperatures, ECS Transactions 11 (2007) 543.
[35] J. Mishler, Y. Wang, P.P. Mukherjee, R. Mukundan, R.L. Borup, Subfreezing operation of polymer electrolyte fuel cells: Ice formation and cell performance loss, Electrochimica Acta 65 (2012) 127.
[36] J.H. Nam, M. Kaviany, Effective diffusivity and water-saturation distribution in single-and twolayer PEMFC diffusion medium, International Journal of Heat and Mass Transfer 46 (2003) 4595.
[37] J.H. Nam, K.J. Lee, G.S. Hwang, C.J. Kim, M. Kaviany, Microporous layer for water morphology control in PEMFC, International Journal of Heat and Mass Transfer 52 (2009) 2779.
[38] R. Alink, D. Gerteisen, W. Merida, Investigating the water transport in porous media for PEMFCs by liquid water visualization in ESEM, Fuel Cells 11 (2011) 481.
[39] F. Garzon, J. Davey, R. Borup, Fuel cell catalyst particle size growth characterized by x-ray scattering methods, ECS Transactions 1 (2006) 153.